AIAA SciTech Forum
6-10 January 2020, Orlando, FL
AIAA Scitech 2020 Forum

10.2514/6.2020-1752



# An Enriched Basis Discontinuous Galerkin Method for Shocks and High-Gradient Features in Fluid Mechanics

Steven R. Brill*
*Institute for Computational and Mathematical Engineering, Stanford University, Stanford, CA, 94305, United States*

Matthias Ihme†
*Department of Mechanical Engineering, Stanford University, Stanford, CA, 94305, United States*

**Discontinuous Galerkin methods struggle to efficiently represent high-gradient features without spurious oscillations due to their polynomial basis. This paper discusses the development of an enriched basis discontinuous Galerkin method to better resolve high-gradient features in compressible flows. The standard polynomial basis is augmented with problem-specific non-polynomial enrichment functions to represent underresolved features. The enrichment functions are incorporated into the basis using a partition of unity to keep the methodology consistent. The method was tailored for shock capturing and wall-modeling of turbulent flows. The performance is evaluated with shock tube problems and Reynolds-averaged Navier-Stokes turbulent channel simulations. The results show this methodology allows for sharp representation of shocks within elements and for larger elements and fewer degrees of freedom to be used in the near wall region of turbulent channel flows.**



## I. Introduction

Throughout fluid mechanics, high-order discontinuous Galerkin (DG) methods have shown advantages over conventional second-order finite volume schemes [1]. Some such advantages of DG schemes are geometric flexibility, high spatial order of accuracy, a high degree of scalability, and flexibility for representing the solution via *hp*-adaptability. DG methods have demonstrated success in a wide range of areas such as aerodynamics [2], turbulence [3], combustion [4], and hypersonic reentry [5].

While DG methods have had success in many areas, they struggle to efficiently represent shocks and other high-gradient features, such as boundary layers, contacts, or reaction fronts. This is a consequence of the polynomial basis on which DG methods are developed, which is subject to spurious oscillations and instabilities. For shocks, a number of different techniques, such as limiters [6] [7], artificial viscosity [8], and mesh optimization methods [9], have been developed, but none have presented a clear solution to the issues presented because they can cause a loss of accuracy, smoothing of shocks, and a great increase in computational cost. In order to resolve turbulent boundary layers, meshes in which wall normal resolution scales with $Re_\tau^2$ in the near-wall region must be used [10]. There has been work done to develop wall-models for DG methods following the work in the finite volume and finite difference communities, but these methods become insufficient for application to higher Reynolds number flows [11] [12] or require modifications to the DG algorithm [13].

In this paper, we present another type of method to better represent shocks and boundary layers in DG methods using basis enrichment. In this method, problem dependent, non-polynomial enrichment functions that represent high-gradient features are added to the solution basis. This method does not require that the enrichment functions are used in the solution representation, but allows the method to choose these degrees of freedom to represent the solution if they improve the solution. The theoretical details of this methodology were developed for continuous finite elements in the partition-of-unity method (PUM) [14] and have been developed further in the extended finite element method (XFEM) and the generalized finite element method (GFEM) [15]. While these methods were originally developed for crack propagation and solid mechanics applications, they have since been applied to high-gradient convection-diffusion equations [16] and Stokes flows [17]. Additionally, this framework was combined with DG methods for high Péclet number advection-diffusion problems [18], two-phase flows [19], immersed boundary methods [20], and recently for RANS [21] and hybrid RANS/LES simulations of incompressible, wall-bounded turbulent flows [22]. However, to our knowledge, there has been little work done to apply enriched basis methods to compressible flows. By addressing this

*srbrill@stanford.edu
†mihme@stanford.edu

issue, we have adapted basis enrichment methods from the finite element community to a DG framework to improve the resolution of shocks and boundary layers in compressible flow simulations. This study serves as an initial test of the potential of enriched basis methods for shock-capturing and wall-modeling of compressible flows. As such, an emphasis was placed on simplicity of the methods developed and further steps will be taken to optimize the methods for the chosen applications in the future.

## II. Mathematical Formulation

This section describes the governing equations, discontinuous Galerkin discretization, and enriched basis discontinuous Galerkin framework.

### A. Compressible Flow Governing Equations

The first set of governing equations considered in this study is the compressible Navier-Stokes equations with the equations for conservation of mass, momentum, and total internal energy written as

$$\partial_t \rho + \nabla \cdot (\rho \boldsymbol{u}) = 0, \tag{1}$$

$$\partial_t (\rho \boldsymbol{u}) + \nabla \cdot (\rho \boldsymbol{u} \otimes \boldsymbol{u} + p\boldsymbol{I}) = \nabla \cdot \boldsymbol{\tau}, \tag{2}$$

$$\partial_t (\rho E) + \nabla \cdot (\boldsymbol{u}(\rho E + p)) = \nabla \cdot (\boldsymbol{u} \cdot \boldsymbol{\tau}) - \nabla \cdot \boldsymbol{q}, \tag{3}$$

where $t$ is time, $\rho$ is density, $\boldsymbol{u}$ is velocity, $p$ is pressure, $E$ is total energy, $\boldsymbol{\tau}$ is the Reynolds stress, and $\boldsymbol{q}$ is the heat flux. The ideal gas law is used to relate pressure to total energy as

$$p = (\gamma - 1)\left(\rho E - \frac{\rho}{2}|\boldsymbol{u}|^2\right), \tag{4}$$

where $\gamma$ is the ratio of specific heats, which is set to a constant value of 1.4 in this study. The Reynolds stress and heat flux are defined as

$$\boldsymbol{\tau} = \mu(\nabla \boldsymbol{u} + (\nabla \boldsymbol{u})^T - \frac{2}{3}(\nabla \cdot \boldsymbol{u})\boldsymbol{I}), \tag{5}$$

$$\boldsymbol{q} = k \nabla T, \qquad k = \frac{C_p \mu}{Pr}, \tag{6}$$

where $\mu$ is the dynamic viscosity, $T$ is the temperature, $C_p$ is the specific heat at constant pressure, and $Pr$ is the Prandtl number. The Euler equations are the simplified case of the compressible Navier-Stokes equations when $\mu = 0$.

The second set of governing equations is the Reynolds-Averaged Navier-Stokes (RANS) equations closed with the Spalart-Allmaras (SA) turbulence model [23], where we consider the Eqs. (1)-(3) with the additional transport equation for the turbulent working variable, $\tilde{\nu}$:

$$\partial_t (\rho \tilde{\nu}) + \nabla \cdot (\rho \boldsymbol{u} \tilde{\nu}) = \nabla \cdot \left(\frac{\eta}{\sigma} \nabla \tilde{\nu}\right) + \frac{c_{b2}\rho}{\sigma} \nabla \tilde{\nu} \cdot \nabla \tilde{\nu} + \mathcal{P} - \mathcal{D}. \tag{7}$$

For the RANS equations, Reynolds stress and heat flux are

$$\boldsymbol{\tau} = (\mu + \mu_t)(\nabla \boldsymbol{u} + (\nabla \boldsymbol{u})^T - \frac{2}{3}(\nabla \cdot \boldsymbol{u})\boldsymbol{I}), \tag{8}$$

$$\boldsymbol{q} = (k + k_t)\nabla T, \qquad k_t = \frac{C_p \mu_t}{Pr_t}, \tag{9}$$

where the eddy viscosity, $\mu_t$, is defined as

$$\mu_t = \begin{cases} \rho \tilde{\nu} f_{v1} & \tilde{\nu} \geq 0 \\ 0 & \tilde{\nu} < 0 \end{cases}, \qquad f_{v1} = \frac{\chi^3}{\chi^3 + c_{v1}^3}, \quad \chi = \frac{\tilde{\nu}}{\nu}. \tag{10}$$

The SA working variable has a viscosity given by $\eta/\sigma$ where

$$\eta = \begin{cases} \mu(1 + \chi) & \chi \geq 0 \\ \mu(1 + \chi + \chi^2) & \chi < 0 \end{cases}. \tag{11}$$

The production and destruction terms, $\mathcal{P}$ and $\mathcal{D}$, are given by

$$\mathcal{P} = \begin{cases} c_{b1}\widetilde{S}\rho\tilde{\nu} & \chi \geq 0 \\ c_{b1}S\rho\tilde{\nu}g_n & \chi < 0 \end{cases}, \qquad \widetilde{S} = \begin{cases} S + \bar{S} & \bar{S} \geq -c_{v2}S \\ S + \dfrac{S(c_{v2}^2 S + c_{v3}\bar{S})}{(c_{v3} - 2c_{v2})S - \bar{S}} & \bar{S} < -c_{v2}S \end{cases}, \tag{12}$$

$$\mathcal{D} = \begin{cases} c_{w1}f_w \dfrac{\rho\tilde{\nu}^2}{d^2} & \chi \geq 0 \\ -c_{w1}\dfrac{\rho\tilde{\nu}^2}{d^2} & \chi < 0 \end{cases}, \tag{13}$$

where $S = \sqrt{\boldsymbol{\omega}\cdot\boldsymbol{\omega}}$ is the vorticity magnitude, the vorticity is $\boldsymbol{\omega} = \nabla \times \boldsymbol{u}$, and

$$g_n = 1 - \frac{1000\chi^2}{1+\chi^2}, \qquad \bar{S} = \frac{\tilde{\nu}f_{v2}}{\kappa^2 d^2}, \qquad f_{v2} = 1 - \frac{\chi}{1+\chi f_{v1}}, \tag{14}$$

$$f_w = g\left(\frac{1+c_{w3}^6}{g^6 + c_{w3}^6}\right)^{1/6}, \qquad g = r + c_{w2}(r^6 - r), \qquad r = \frac{\tilde{\nu}}{\widetilde{S}\kappa^2 d^2}. \tag{15}$$

Finally, the closure coefficients are $\sigma = 2/3$, $\kappa = 0.41$, $Pr_t = 0.9$, $c_{b1} = 0.1355$, $c_{b2} = 0.622$, $c_{w1} = \dfrac{c_{b1}}{\kappa^2} + \dfrac{1+c_{b2}}{\sigma}$, $c_{w2} = 0.3$, $c_{w3} = 2$, $c_{v1} = 7.1$, $c_{v2} = 0.7$, and $c_{v3} = 0.9$.

Equations (1)-(3) and (7) can be written in vector form as

$$\partial_t \mathbf{U} + \nabla\cdot\mathbf{F} = \nabla\cdot\mathbf{Q} + \mathbf{S}, \tag{16}$$

where $\mathbf{U}(\boldsymbol{x},t) : \mathbb{R}^{N_d}\times\mathbb{R} \to \mathbb{R}^{N_U}$ is the conservative state vector, $\mathbf{F}(\boldsymbol{U}) : \mathbb{R}^{N_U} \to \mathbb{R}^{N_U\times N_d}$ is the inviscid flux vector, $\mathbf{Q}(\boldsymbol{U}) : \mathbb{R}^{N_U} \to \mathbb{R}^{N_U\times N_d}$ is the viscous flux vector, $\mathbf{S} \in \mathbb{R}^{N_U}$ is the source term vector, $\boldsymbol{x} \in \mathbb{R}^{N_d}$ is the spatial coordinate vector, $N_U$ is the number of state variables, and $N_d$ is the number of spatial dimensions.

### B. Discontinuous Galerkin Discretization

In a discontinuous Galerkin framework, the problem is posed on a computational domain, $\Omega$ with a boundary $\partial\Omega$. $\Omega$ is partitioned into $N_e$ non-overlapping discrete elements such that $\Omega = \cup_{e=1}^{N_e}\Omega_e$. The boundary of element $\Omega_e$ is denoted by $\partial\Omega_e$. The global space of test functions is defined as

$$\mathcal{V} = \oplus_{e=1}^{N_e}\mathcal{V}_e, \qquad \mathcal{V}_e = \text{span}\{\phi_n^e(\Omega_e)\}_{n=1}^{N_b^e}, \tag{17}$$

where $\phi_n^e$ is the $n$th basis function on element $e$ and $N_b^e$ is the number of basis functions on element $e$. The global solution $\mathbf{U}$ is approximated by $\boldsymbol{U}$, where

$$\boldsymbol{U} = \oplus_{e=1}^{N_e}\boldsymbol{U}^e, \qquad \boldsymbol{U}^e \in \mathcal{V}_e. \tag{18}$$

For a traditional DG method, the basis functions for each element are $P$th order polynomials. The local solution approximation on an element $e$, $\boldsymbol{U}^e$ is given by

$$\boldsymbol{U}^e(\boldsymbol{x},t) = \sum_{m=1}^{N_b^e}\widetilde{\boldsymbol{U}}_m^e(t)\phi_m^e(\boldsymbol{x}), \tag{19}$$

where $\widetilde{\boldsymbol{U}}_m^e(t)$ is the vector of basis coefficients at time $t$. The local weak form of the governing equations is created by multiplying Eq. (16) by the $n$th test function and integrating over the element

$$\int_{\Omega_e}\phi_n^e\partial_t\mathbf{U}^e\,d\Omega_e + \int_{\Omega_e}\phi_n^e\nabla\cdot\mathbf{F}\,d\Omega_e = \int_{\Omega_e}\phi_n^e\nabla\cdot\mathbf{Q}\,d\Omega_e + \int_{\Omega_e}\phi_n^e\mathbf{S}\,d\Omega_e, \qquad \forall\phi_n^e, n = 1,\ldots,N_b^e. \tag{20}$$

Then, the weak form is discretized to solve for the basis coefficients. The LHS of Eq. (20) is discretized by letting $\boldsymbol{F}$ be an approximation to $\mathbf{F}$ and integrating Eq. (20) by parts to yield

$$\int_{\Omega_e} \phi_n^e \partial_t \mathbf{U}^e \, d\Omega_e + \int_{\Omega_e} \phi_n^e \nabla \cdot \mathbf{F} \, d\Omega_e = \int_{\Omega_e} \left( \phi_n^e \partial_t \mathbf{U}^e - \nabla \phi_n^e \cdot \mathbf{F} \right) d\Omega_e + \oint_{\partial\Omega_e} \phi_n^e \mathbf{F} \cdot \hat{\mathbf{n}} \, d\Gamma_e \tag{21}$$

$$\approx \sum_{m=1}^{N_b^e} d_t \widetilde{\boldsymbol{U}}_m^e(t) \int_{\Omega_e} \phi_n^e \phi_m^e \, d\Omega_e - \int_{\Omega_e} \nabla \phi_n^e \cdot \boldsymbol{F} \, d\Omega_e + \oint_{\partial\Omega_e} \phi_n^{e+} \widehat{\boldsymbol{F}} \, d\Gamma_e, \tag{22}$$

where $\hat{\mathbf{n}}$ is the outward pointing normal on $\partial\Omega_e$ and the notation $(\cdot)^+$ and $(\cdot)^-$ refer to the interior and exterior information about element $\Omega_e$, respectively. $\widehat{\boldsymbol{F}}$ is the inviscid numerical flux used to couple adjacent elements, which is chosen to be the Roe flux [24] in this study.

The discretization of the viscous flux is described by letting $\mathbf{Q}_i \in \mathbb{R}^{N_d}$ be the linearized diffusion flux of the $i$th state variable such that

$$\mathbf{Q}_i = \mathbf{D}_i : \nabla \mathbf{U} \tag{23}$$

$$= \sum_{k=1}^{N_U} \mathbf{D}_{ik} \nabla \mathrm{U}_k, \tag{24}$$

where $\mathbf{D} \in \mathbb{R}^{N_U \times N_U \times N_d \times N_d}$ is a fourth-order tensor for the first-order differentiation of the viscous flux with respect to the solution gradient. Then for simplicity, $\mathbf{Q}_i^k = \mathbf{D}_{ik} \nabla U_k$ is discretized and then summed to compute its contribution to Eq. (20). Note that for every $i$ and $k$, $\mathbf{Q}_i^k \in \mathbb{R}^{N_d}$, $\mathbf{D}_{ik} \in \mathbb{R}^{N_d \times N_d}$, and $\nabla U_k \in \mathbb{R}^{N_d}$. Approximating $\mathbf{Q}$ and $\mathbf{D}$ as $\boldsymbol{Q}$ and $\boldsymbol{D}$ respectively, the discretization of $\nabla \cdot \mathbf{Q}_i^k$ is

$$\int_{\Omega_e} \phi_n^e \nabla \cdot \mathbf{Q}_i^k \, d\Omega_e = -\int_{\Omega_e} \nabla \phi_n^e \cdot (\mathbf{D}_{ik} \nabla \mathrm{U}_k) \, d\Omega_e + \oint_{\partial\Omega_e} \phi_n^e \mathbf{Q}_i^k \cdot \widehat{\boldsymbol{n}} \, d\Gamma_e \tag{25}$$

$$= \int_{\Omega_e} U_k \nabla \cdot \left( \mathbf{D}_{ik}^T \nabla \phi_n^e \right) d\Omega_e - \oint_{\partial\Omega_e} \mathrm{U}_k \left( \mathbf{D}_{ik}^T \nabla \phi_n^e \right) \cdot \widehat{\boldsymbol{n}} \, d\Gamma_e + \oint_{\partial\Omega_e} \phi_n^e \mathbf{Q}_i^k \cdot \widehat{\boldsymbol{n}} \, d\Gamma_e \tag{26}$$

$$\approx \int_{\Omega_e} U_k \nabla \cdot \left( \boldsymbol{D}_{ik}^T \nabla \phi_n^e \right) d\Omega_e - \oint_{\partial\Omega_e} \widehat{U}_k \left( \boldsymbol{D}_{ik}^T \nabla \phi_n^e \right)^+ \cdot \widehat{\boldsymbol{n}} \, d\Gamma_e + \oint_{\partial\Omega_e} \phi_n^{e+} \widehat{\boldsymbol{Q}}_i^k \, d\Gamma_e \tag{27}$$

$$= -\int_{\Omega_e} \nabla \phi_n^e \cdot \left( \boldsymbol{D}_{ik}^T \nabla U_k \right) d\Omega_e + \oint_{\partial\Omega_e} \left( U_k^+ - \widehat{U}_k \right) \left( \boldsymbol{D}_{ik}^T \nabla \phi_n^e \right)^+ \cdot \widehat{\boldsymbol{n}} \, d\Gamma_e + \oint_{\partial\Omega_e} \phi_n^{e+} \widehat{\boldsymbol{Q}}_i^k \, d\Gamma_e. \tag{28}$$

The three terms from the left to the right on the RHS of Eq. (28) represent interior diffusion, dual consistency, and inter-element viscous effects. In this study, $\widehat{\mathbf{U}} = \{\mathbf{U}\}$, where the operator $\{\cdot\} \coloneqq \frac{1}{2}[(\cdot)^+ + (\cdot)^-]$ is the mean value across element faces, and the definition of $\widehat{\boldsymbol{Q}}_i$ is the well-known BR2 scheme [25].

### C. Enriched Basis Discontinuous Galerkin Method

In order to better represent unresolved features, such as shocks and boundary layers, and to avoid oscillations around discontinuities, the polynomial basis was enriched by adding non-polynomial enrichment functions to the basis through the use of the partition of unity [14]. The partition of unity consists of a set of $N_m$ polynomials, $\varphi_n$. For this study, both the polynomial basis and the partition of unity are chosen to be the same set of Lagrange polynomials, but in general this is not necessary. With the additional enrichment functions, the approximation of the solution becomes

$$\boldsymbol{U}^e(\boldsymbol{x}, t) = \sum_{m=1}^{N_p^e} \widetilde{\boldsymbol{U}}_m^e(t) \phi_m^e(\boldsymbol{x}) + \sum_{n=1}^{N_m^e} \widetilde{\boldsymbol{a}}_n^e(t) \varphi_n^e(\boldsymbol{x}) \psi^e(\boldsymbol{x}) = \sum_{m=1}^{N_b^e} \widetilde{\boldsymbol{V}}_m^e(t) \Phi_m^e(\boldsymbol{x}), \tag{29}$$

where $N_p^e$ is the number of polynomial basis functions in element $e$, $\psi^e(\boldsymbol{x})$ is the local enrichment function in the element $e$, and $\widetilde{\boldsymbol{V}}_m^e$ and $\Phi_m^e$ are the combined coefficients and basis functions:

$$\Phi^e = [\phi_1^e, ..., \phi_{N_p^e}^e, \varphi_1^e \psi^e, ..., \varphi_{N_m^e}^e \psi^e], \tag{30}$$

$$\widetilde{\boldsymbol{V}^e} = [\widetilde{\boldsymbol{U}}_1^e, ..., \widetilde{\boldsymbol{U}}_{N_p^e}^e, \widetilde{\boldsymbol{a}}_1^e, ..., \widetilde{\boldsymbol{a}}_{N_m^e}^e]. \tag{31}$$

Note that now $N_b^e = N_p^e + N_m^e$. The enrichment function is defined locally, because it can be chosen to be a global function that enriches each element differently or a local function that enriches every element the same. Adding enrichment functions only modifies the basis on each individual element, so the coefficients are found using the discretized weak solution similar to Eq. (20):

$$\sum_{m=1}^{N_b^e} d_t \widetilde{\boldsymbol{V}}_m^e(t) \int_{\Omega_e} \Phi_n^e \Phi_m^e \, d\Omega_e + \int_{\Omega_e} \Phi_n^e \nabla \cdot \boldsymbol{F} \, d\Omega_e = \int_{\Omega_e} \Phi_n^e \nabla \cdot \boldsymbol{Q} \, d\Omega_e + \int_{\Omega_e} \Phi_n^e \boldsymbol{S} \, d\Omega_e, \qquad \forall \Phi_n^e, n = 1, ..., N_b^e. \quad (32)$$

As in the standard DG method, the variational form is integrated by parts and a numerical flux is used to couple the elements.

The choice of enrichment function is problem specific and it is chosen to be a function that includes a feature that the polynomial basis cannot represent. For example, for a turbulent boundary layer problem, the law of the wall could be used in the elements at the wall. For a shock, a Heaviside function or hyperbolic tangent could be used. The enrichment modes in the solution basis do not enforce that the solution uses these modes, but rather give the method the option to use them when the Galerkin procedure determines them optimal. Hence the formulation remains consistent.

The enriched DG method only changes the basis, so the algorithm is exactly the same as classical DG but with non-polynomial basis functions. Because the enrichment functions and enriched basis functions are not polynomials, the standard $2P + 1$ Gauss-Legendre quadrature points, where $P$ is the polynomial order of the basis functions, are no longer sufficient when integrating the weak form. Hence additional quadrature rules must be designed for the chosen enrichment functions. In this study, all elements are tensor-product elements with the chosen enrichment functions defined as piecewise functions aligned with one of the reference directions. To numerically integrate these functions, the reference space is split along the piecewise interval boundaries in the direction of the enrichment function, a sufficient number of Gauss-Legendre quadrature points is used to integrate each interval, and the results are summed:

$$\int_{-1}^{1} \psi(\xi) \, d\xi = \int_{-1}^{\xi_1} \psi(\xi) \, d\xi + \int_{\xi_1}^{\xi_2} \psi(\xi) \, d\xi + ... \int_{\xi_k}^{1} \psi(\xi) \, d\xi, \quad (33)$$

where $k$ is the number of pieces in the enrichment function. The specific enrichment orders and segments for the enrichment functions will be detailed along with the definition of the enrichment functions in the discussions of the results.

In the case of a discontinuous enrichment function, the formulation of the discretized equations must be modified to account for the discontinuity. We will consider an enrichment function $\psi^e(\boldsymbol{x}) = g^e(\boldsymbol{x}) \, H(L(\boldsymbol{x}, \mathcal{J}^e))$ where $g^e$ is a continuous function on element $e$, $H$ is the Heaviside step function, and $L(\boldsymbol{x}, \mathcal{J}^e)$ is a signed distance level set function from a surface $\mathcal{J}^e$ that defines where the discontinuity occurs in element $e$. The signed distance level set function is defined as:

$$L(\boldsymbol{x}, \mathcal{J}^e) = \text{sign}(\widehat{\boldsymbol{n}} \cdot (\boldsymbol{x} - \boldsymbol{x}^*)) \min_{\boldsymbol{x}^* \in \mathcal{J}^e} \|\boldsymbol{x} - \boldsymbol{x}^*\|, \quad (34)$$

where $\widehat{\boldsymbol{n}}$ is the unit normal to $\mathcal{J}^e$. Using split quadrature around the discontinuity will accurately integrate the discontinuous enrichment function. However, when integrating Eq. (32) by parts for the enriched basis functions, the gradient of the Heaviside function is a delta function which cannot be resolved with numerical integration over the element. The discontinuity within the element is equivalent to a cut-cell and thus is treated with a numerical flux that is integrated across the surface $\mathcal{J}^e$:

$$\int_{\Omega_e} \varphi_n^e \psi^e \nabla \cdot \boldsymbol{F} \, d\Omega_e = \int_{\Omega_e} \varphi_n^e g^e H(L(\boldsymbol{x}, \mathcal{J}^e)) \nabla \cdot \boldsymbol{F} \, d\Omega_e \quad (35)$$

$$= -\int_{\Omega_e} \nabla \cdot (\varphi_n^e g^e) H(L(\boldsymbol{x}, \mathcal{J}^e)) \boldsymbol{F} \, d\Omega_e - \oint_{\mathcal{J}^e} \varphi_n^e g^e \widehat{\boldsymbol{F}} \, d\mathcal{J}^e + \oint_{\partial\Omega_e} (\varphi_n^e g^e H(L(\boldsymbol{x}, \mathcal{J}^e)))^+ \widehat{\boldsymbol{F}} \, d\Gamma_e. \quad (36)$$

In this study, discontinuous enrichment functions were only used with the Euler equations, so only the inviscid flux is considered. For the case of a 1-D problem with an enrichment function $\psi^e(x) = g^e(x) H(x - x^{e*})$, where $x^{e*}$ is the

location of discontinuity, the notation simplifies to

$$\int_{\Omega_e} \varphi_n^e \psi^e \frac{\partial}{\partial x} \boldsymbol{F}\, d\Omega_e = \int_{\Omega_e} \varphi_n^e g^e H(x - x^{e*}) \frac{\partial}{\partial x} \boldsymbol{F}\, d\Omega_e \tag{37}$$

$$= -\int_{\Omega_e} \frac{\partial}{\partial x}(\varphi_n^e g^e) H(x - x^{e*}) \boldsymbol{F}\, d\Omega_e - \left[\varphi_n^e g^e \widehat{\boldsymbol{F}}\right]\Big|_{x=x^{e*}} + \oint_{\partial\Omega_e} (\varphi_n^e g^e H(x - x^{e*}))^+ \widehat{\boldsymbol{F}}\, d\Gamma_e. \tag{38}$$

## III. Numerical Results

In this section, we will present numerical results from two different types of tests: 1-D shock tube problems and RANS simulations of turbulent channel flows. The problem is defined, the choice of enrichment function and quadrature rule is discussed, and numerical results are presented in comparison with conventional methods.

### A. Stationary Shock Problem

The polynomial basis of standard DG methods makes them unable to represent the discontinuity that occurs at a shock without smoothing the shock or causing oscillations in the solution. The enriched basis serves as a way to introduce a step function into the basis to better capture the discontinuous profile of the shock and reduce the oscillations. First, a stationary shock tube problem was studied. The shock is initialized at $x = 0.51$ with the left and right states defined as

$$\rho_L = 1 \qquad u_L = 1 \qquad P_L = 0.044642, \tag{39}$$

$$\rho_R = 4.5714 \qquad u_R = 0.21875 \qquad P_R = 0.82589, \tag{40}$$

and the left and right boundaries set to the appropriate initial state. These conditions create a Mach 4 shock that stays stationary in its initial location due to uniform fluxes across the shock. The domain of $x \in [0, 1]$ was discretized with 50 $P = 1$ Lagrange polynomial elements, which puts the shock in the center of the center element. The Heaviside step function defined at the center of the element in reference space was used as the enrichment function in each element:

$$\psi(\xi) = H(\xi) = \begin{cases} 0 & \text{if } \xi < 0 \\ 1 & \text{otherwise} \end{cases}, \qquad \xi \in [-1, 1]. \tag{41}$$

For this enrichment function, the quadrature must be split at the discontinuity and a numerical flux must be computed at $\xi = 0$ as detailed in Eq. (38). Because the enrichment function is constant on each side the discontinuity, the standard $2P + 1$ quadrature points can be used on each subdomain:

$$N_q = \begin{cases} 2P + 1 & \text{for } \xi \in [-1, 0] \\ 2P + 1 & \text{for } \xi \in [0, 1] \end{cases}. \tag{42}$$

4th-order Runge-Kutta was used for time integration and the solution was advanced until time $t = 5$.

The results in Figure 1 show that the method is able to nearly exactly reproduce the exact solution and maintain it as the solution is evolved in time. The standard DG method is unstable for this problem due to undershoots in the polynomial solution causing unphysical quantities. Thus, the enriched DG method can improve the representation of shocks by creating a discontinuous solution at the location of the shock which can stabilize the solution of high Mach number problems that standard DG cannot handle without the addition of limiters or artificial viscosity.

### B. Sod Problem

While the stationary shock problem showed that applying enrichment at the exact location of the shock shows great improvement in the solution, the Sod problem examines how the method performs with a moving shock that is not always aligned with the enrichment functions. The Sod shock tube problem is a 1-D shock tube problem with the diaphragm at $x = 0$ and the left and right states defined as

$$\rho_L = 1 \qquad u_L = 0 \qquad P_L = 1, \tag{43}$$

$$\rho_R = 0.125 \qquad u_R = 0 \qquad P_R = 0.1, \tag{44}$$

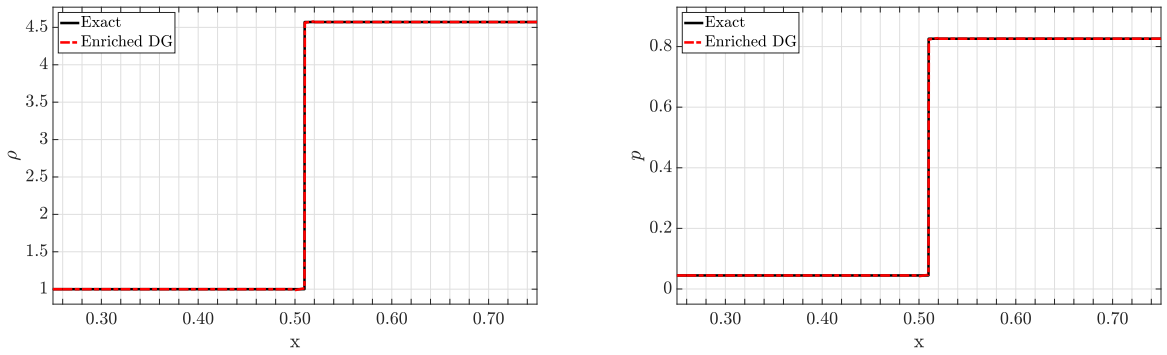


**Fig. 1 Mach 4 stationary shock solution with 50 $P = 1$ elements enriched by a Heaviside step function at the center of each element. The shock is located at $x = 0.51$. Undershoots in standard DG cause unphysical solution for this case.**

and a domain $x \in [-0.5, 0.5]$. The left and right boundary conditions fix the solution at the appropriate initial state. The spatial discretization employs 20 $P = 1$ Lagrange polynomial elements. The enrichment function is the Heaviside step function defined at the center of each element as in the previous case. 4th-order Runge-Kutta was used to integrate in time until $t = 0.15$.

The results in Figure 2 show that the enriched method is able to represent a sharper shock than the standard DG method of the same polynomial order. Because the enrichment function is applied in the center of every element and the shock is moving through the domain, the enrichment function will not always align with the shock in the solution, so one would not expect as good of agreement as was seen in the stationary shock case. However, we still see fewer oscillations in the post-shock region compared to standard DG. Hence, the enriched method shows both a better shock representation and fewer oscillations, despite the misalignment between the shock and enrichment functions. Future work will include developing robust methods to track the location of shocks and modify the enrichment basis in time in order to apply the enrichment function at the exact location of the shock throughout the time advancement of the simulation.

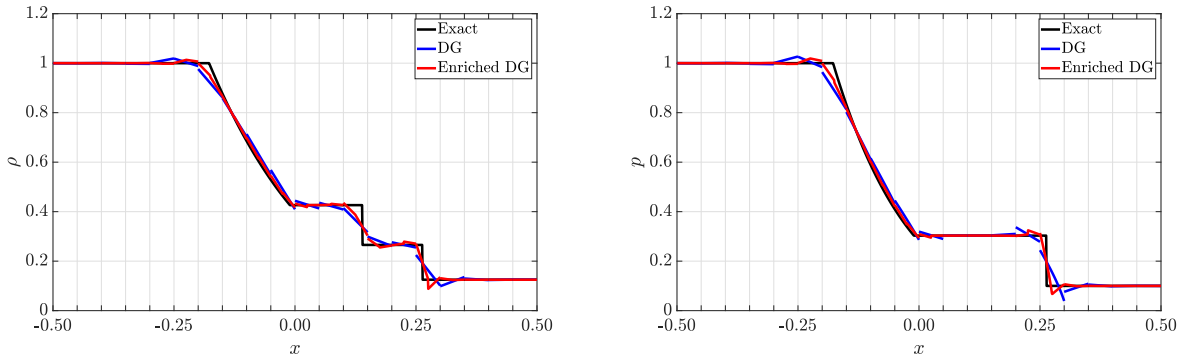


**Fig. 2 Sod problem density and pressure with 20 $P = 1$ elements comparing standard DG solution with DG enriched by a Heaviside step function in the center of each element. Solution is shown at time $t = 0.15$.**

### C. RANS Turbulent Boundary Layer

For turbulent boundary layers, enrichment allows the use of larger elements to represent the boundary layer. Normally, in order to fully resolve the momentum boundary layer, grid resolution on the order of $Re_\tau^2$ is necessary to accurately predict the mean velocity profile. To avoid the added computational costs associated with this mesh refinement, we enrich the wall-adjacent elements with a law of the wall enrichment function. The law of the wall is a self-similar solution for the wall-parallel velocity in the near wall region. It is formed by considering the friction velocity $u_\tau = \sqrt{\frac{\tau_w}{\rho}}$

with $\tau_w = \mu \frac{du}{dy}$ where $y$ is the wall-normal direction. When nondimensionalizing the wall parallel velocity and wall normal distance with the friction velocity, we obtain $u^+ = \frac{u}{u_\tau}$ and $y^+ = \frac{y u_\tau}{\nu}$. The law of the wall is characterized by three different regions: the viscous sublayer, $0 < y^+ < 5$, where $u^+ = y^+$, the buffer layer, $5 < y^+ < 30$, where there is no similarity solution, and the log layer $30 < y^+$ where $u^+ = \frac{1}{\kappa} \log(y^+) + \beta$. In order to represent this steep profile with large elements, an enrichment function containing the law of the wall is defined as

$$\psi(\boldsymbol{x}) = \psi_w(\boldsymbol{x}) = \begin{cases} y^+ & \text{if } y^+ \leq y^{+*} \\ \frac{1}{\kappa} \log(y^+) + \beta & \text{if } y^+ > y^{+*} \end{cases}, \tag{45}$$

where $y^{+*}$ corresponds to the point where the viscous sublayer and the log layer profiles are equal, so the enrichment function is continuous. In this enrichment function, $\kappa$, $\beta$, $u_\tau$, and $\nu$ are set using a priori knowledge and are kept constant throughout the simulation. Other law of the wall functions could be chosen as the enrichment function, but this function was chosen because of its simplicity. Due to the kink in the enrichment function at $y^+ = y^{+*}$, split quadrature must be used to accurate integrate this enrichment function and its derivative. Using tensor-product elements, the standard $2P + 1$ quadrature points was used in the wall-parallel directions and split quadrature was used in the wall normal direction. The quadrature in the wall normal direction is defined as

$$N_q = \begin{cases} 2(P+1)+1 & \text{for } \xi \in [-1, \xi_{y^{+*}}] \\ 2(P+5)+1 & \text{for } \xi \in [\xi_{y^{+*}}, 1] \end{cases}, \tag{46}$$

where $\xi_{y^{+*}}$ is the reference space location of $y^{+*}$. Two additional quadrature points are needed to exactly integrate the linear region. 10 additional quadrature points was experimentally determined to integrate the log-layer well. To effectively use this enrichment function, the entire law of the wall region ($y^+ < 40$) must be contained in a single element. If too small of elements are enriched, the polynomial modes will span a similar space to the enriched modes and the mass matrix will be ill-conditioned. Also, only the wall-adjacent elements will be enriched, because outside of the near-wall region, the solution is sufficiently smooth so the enrichment is not necessary.

For this case, we have chosen to apply this law of the wall enrichment to RANS simulations of a turbulent channel. The SA model was chosen to model the unclosed terms in the equations, due to its simplicity and use in DG contexts [26]. The domain of size $[0, 2\pi] \times [0, 2]$ was discretized with $N$ uniform quadrilateral elements in each direction. The polynomial bases were order $P$ uniform Lagrange polynomials. The solution was advanced in time using BDF2 for 25 flow through times. The boundary conditions are periodic in $x$ and isothermal cold walls in $y$ are used with a Mach number of $M = 0.1$. The channel is forced with a constant pressure gradient of 1, the initial density is set to $\rho = 1$, and the viscosity is kept constant. As a result, the steady-state solution gives $u_\tau = 1$, so $Re_\tau = \frac{1}{\mu}$ and the dynamic viscosity determines the resulting friction Reynolds number. The enrichment functions were chosen to be $\psi_w$ with $\kappa = 0.41$, $\beta = 5.2$, $u_\tau = 1$, and $\nu = \frac{1}{Re_\tau}$ and were used only in the wall adjacent elements. $Re_\tau = 200$, 590, and 2000 were tested.

The results for the case with $Re_\tau = 200$ illustrated in Figure 3 show that both the standard DG methods with $N = 8$ and $N = 16$ $P = 3$ elements show good agreement with the law of the wall. However, the enriched method is able to produce greater accuracy in the viscous sublayer and similar accuracy in the log-layer with only 4 elements in each direction. Comparing the number of degrees of freedom for each state variable, the enriched method with only 384 degrees of freedom has comparable results to a standard method with 1024 degrees of freedom. For $Re_\tau = 590$, Figure 4 shows that the standard DG method with $N = 16$ and $P = 3$ underpredicts the law of the wall. The enriched method is able to produce similar levels of accuracy as DG $N = 16$ and $P = 4$ with only $N = 4$ and $N = 8$ $P = 3$ elements. The ratio of degrees of freedom between standard and enriched DG is 10:1. For $Re_\tau = 2000$, Figure 5 shows the enriched method is able to predict the law of the wall with only 16 $P = 3$ elements in each direction while the DG solutions underpredict the law of the wall with $N = 64$ and $P = 3$. The enriched method has 14 times fewer degrees of freedom and can better resolve the law of the wall.

In all three cases, the enriched method outperforms the standard method. In the coarsest enriched solutions for each case, the first element spans up to $y^+ = O(100)$, which highlights the ability of the enriched method to represent the law of the wall with coarse elements. Additionally, the comparison of degrees of freedom show that for larger Reynolds numbers, the enriched method can produce similar or better results with less than 10 times fewer degrees of freedom. The reduction in degrees of freedom is due to the fact that only the wall-adjacent elements are enriched, so the number of added degrees of freedom is much smaller than the number of degrees of freedom in the rest of the domain. As $Re_\tau$ increases, the standard DG methods fail to capture the law of the wall and the advantages of the enriched DG methods are shown. Hence the enrichment functions greatly increase the resolution capabilities of the DG method. The next step

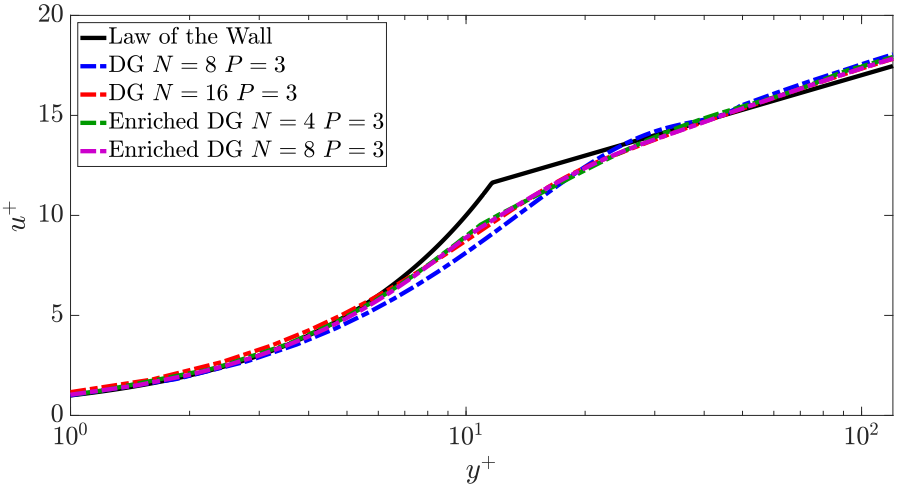


**Fig. 3** $Re_\tau = 200$ **RANS turbulent channel with** $N \times N$ **uniform elements and** $P$ **order basis polynomials. Enriched solutions use a law of the wall enrichment function in the wall-adjacent elements.**

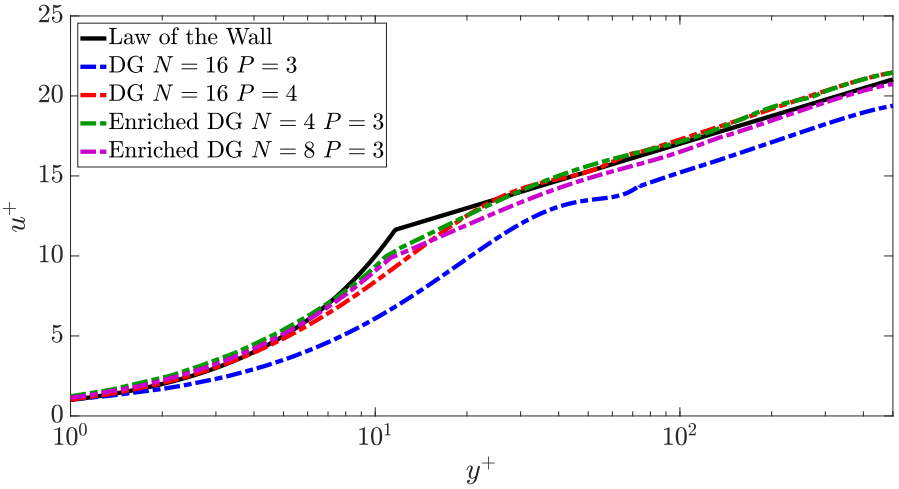


**Fig. 4** $Re_\tau = 590$ **RANS turbulent channel with** $N \times N$ **uniform elements and** $P$ **order basis polynomials. Enriched solutions use a law of the wall enrichment function in the wall-adjacent elements.**



is to extend this method to handle more complex wall-bounded flows than simple channel flows. One key step in this process is incorporating a method to adapt the enrichment function to the local $\tau_w$. Additionally, other enrichment functions can be explored, since this law of the wall was chosen for simplicity. Finally, the method can be applied to fully compressible flows by using a different enrichment function in the energy equation to capture the thermal boundary layer.

## IV. Conclusion

In conclusion, we have developed an enriched basis high-order discontinuous Galerkin method for compressible flows. This method involves incorporating problem-specific non-polynomial enrichment functions that mimic the desired behavior into the solution basis. With this, the solver can take advantage of these basis functions to better represent high-gradient features, such as shocks and boundary layers. Since the method only requires a modification of the basis functions, for continuous enrichment functions the only change that is needed in the standard DG algorithm is to use a different quadrature rule in the numerical integrations to fully incorporate the non-polynomial basis functions. In this

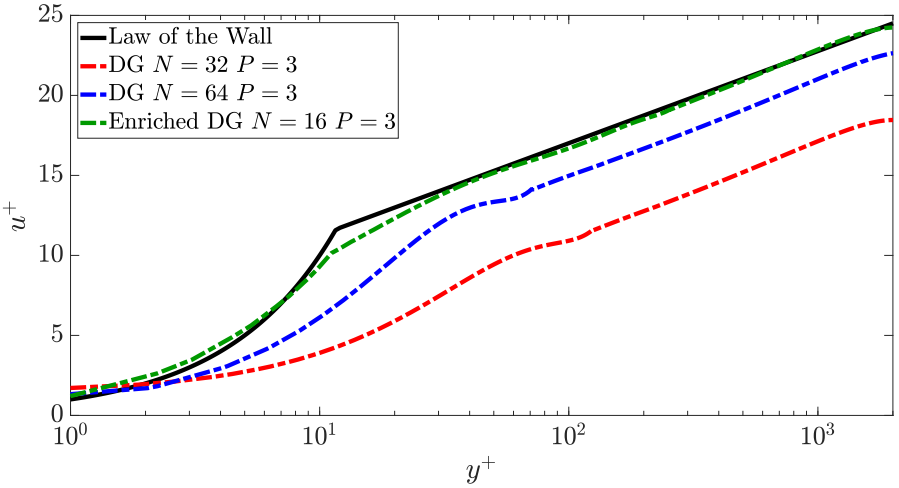


**Fig. 5** $Re_\tau = 2000$ **RANS turbulent channel with** $N \times N$ **uniform elements and** $P$ **order basis polynomials. Enriched solutions use a law of the wall enrichment function in the wall-adjacent elements.**

study, we have found that splitting the reference space in enriched elements along the locations of piecewise interval in the enrichment function and then applying an appropriate number of quadrature points to be an effective quadrature rule. In the case of discontinuous enrichment functions, an additional numerical flux is added to the discretization of the inviscid flux in order to account for the discontinuity.

We have demonstrated the enriched basis discontinuous Galerkin method's potential on 1-D shock tube problems and RANS simulations of turbulent channel flow where it has shown the ability to better represent shocks and represent fully developed boundary layers with much larger elements than traditional methods. Even the simple implementation of constant enrichment functions at fixed locations was able to improve the solutions of these problems, showing the potential for better resolution of the targeted features with more complex schemes, such as updating the enrichment function in time. Ongoing work for enriched methods for shock-capturing involves developing methods to locate and update the location of shocks in the enrichment function. These developments will better resolve 1-D shock tube problems and will help the method handle more complex shock-based problems, like supersonic flows over a cylinder. Ongoing work for turbulent wall-modeling with basis enrichment involves developing the method for large-eddy simulations of wall-bounded turbulent flows by adapting the enrichment functions based on the local shear stress to capture local flow features and exploring other near-wall functions.

## Acknowledgments

Financial support from the Department of Defense (DoD) through the National Defense Science & Engineering Graduate Fellowship (NDSEG) Program and the NASA Early Career Faculty program are gratefully acknowledged.

## References

[1] Wang, Z. J., Fidkowski, K., Abgrall, R., Bassi, F., Caraeni, D., Cary, A., Deconinck, H., Hartmann, R., Hillewaert, K., Huynh, H. T., et al., "High-order CFD methods: current status and perspective," *International Journal for Numerical Methods in Fluids*, Vol. 72, No. 8, 2013, pp. 811–845.

[2] Hartmann, R., Held, J., Leicht, T., and Prill, F., "Discontinuous Galerkin methods for computational aerodynamics—3D adaptive flow simulation with the DLR PADGE code," *Aerospace Science and Technology*, Vol. 14, No. 7, 2010, pp. 512–519.

[3] Lv, Y., Ma, P. C., and Ihme, M., "On underresolved simulations of compressible turbulence using an entropy-bounded DG method: solution stabilization, scheme optimization, and benchmark against a finite-volume solver," *Computers & Fluids*, Vol. 161, 2018, pp. 89–106.

[4] Lv, Y., and Ihme, M., "Discontinuous Galerkin method for multicomponent chemically reacting flows and combustion," *Journal of Computational Physics*, Vol. 270, 2014, pp. 105–137.

[5] Ching, E., Lv, Y., and Ihme, M., "Development of Discontinuous Galerkin method for Hypersonic Heating Prediction," *55th AIAA Aerospace Sciences Meeting*, AIAA 2017-0311, 2017.

[6] Burbeau, A., Sagaut, P., and Bruneau, C.-H., "A problem-independent limiter for high-order Runge–Kutta discontinuous Galerkin methods," *Journal of Computational Physics*, Vol. 169, No. 1, 2001, pp. 111–150.

[7] Lv, Y., and Ihme, M., "Entropy-bounded discontinuous Galerkin scheme for Euler equations," *Journal of Computational Physics*, Vol. 295, 2015, pp. 715–739.

[8] Persson, P.-O., and Peraire, J., "Sub-cell shock capturing for discontinuous Galerkin methods," *44th AIAA Aerospace Sciences Meeting and Exhibit*, AIAA 2006-112, 2006.

[9] Zahr, M. J., and Persson, P.-O., "An optimization-based approach for high-order accurate discretization of conservation laws with discontinuous solutions," *Journal of Computational Physics*, Vol. 365, 2018, pp. 105–134.

[10] Choi, H., and Moin, P., "Grid-point requirements for large eddy simulation: Chapman's estimates revisited," *Physics of Fluids*, Vol. 24, No. 1, 2012, p. 011702.

[11] Frère, A., Carton de Wiart, C., Hillewaert, K., Chatelain, P., and Winckelmans, G., "Application of wall-models to discontinuous Galerkin LES," *Physics of Fluids*, Vol. 29, No. 8, 2017, p. 085111.

[12] Carton de Wiart, C., and Murman, S. M., "Assessment of wall-modeled LES strategies within a discontinuous-Galerkin spectral-element framework," *55th AIAA Aerospace Sciences Meeting*, AIAA 2017-1223, 2017.

[13] Lv, Y., Yang, X. I. A., Park, G. I., and Ihme, M., "Physics-based near-wall turbulence modeling in an enriched discontinuous Galerkin framework," *Proceedings of the Summer Program 2018*, Center for Turbulence Research, 2018, pp. 127–136.

[14] Melenk, J. M., and Babuška, I., "The partition of unity finite element method: basic theory and applications," *Computer Methods in Applied Mechanics and Engineering*, Vol. 139, No. 1-4, 1996, pp. 289–314.

[15] Fries, T.-P., and Belytschko, T., "The extended/generalized finite element method: an overview of the method and its applications," *International Journal for Numerical Methods in Engineering*, Vol. 84, No. 3, 2010, pp. 253–304.

[16] Abbas, S., Alizada, A., and Fries, T.-P., "The XFEM for high-gradient solutions in convection-dominated problems," *International Journal for Numerical Methods in Engineering*, Vol. 82, No. 8, 2010, pp. 1044–1072.

[17] Foucard, L. C., and Vernerey, F. J., "An X-FEM-based numerical–asymptotic expansion for simulating a Stokes flow near a sharp corner," *International Journal for Numerical Methods in Engineering*, Vol. 102, No. 2, 2015, pp. 79–98.

[18] Borker, R., Farhat, C., and Tezaur, R., "A discontinuous Galerkin method with Lagrange multipliers for spatially-dependent advection–diffusion problems," *Computer Methods in Applied Mechanics and Engineering*, Vol. 327, 2017, pp. 93–117.

[19] Kummer, F., "Extended discontinuous Galerkin methods for two-phase flows: the spatial discretization," *International Journal for Numerical Methods in Engineering*, Vol. 109, No. 2, 2017, pp. 259–289.

[20] Geisenhofer, M., Kummer, F., and Müller, B., "A discontinuous Galerkin immersed boundary solver for compressible flows: Adaptive local time stepping for artificial viscosity–based shock-capturing on cut cells," *International Journal for Numerical Methods in Fluids*, Vol. 91, No. 9, 2019, pp. 448–472.

[21] Krank, B., Kronbichler, M., and Wall, W. A., "Wall modeling via function enrichment within a high-order DG method for RANS simulations of incompressible flow," *International Journal for Numerical Methods in Fluids*, Vol. 86, No. 1, 2018, pp. 107–129.

[22] Krank, B., Kronbichler, M., and Wall, W. A., "A multiscale approach to hybrid RANS/LES wall modeling within a high-order discontinuous Galerkin scheme using function enrichment," *International Journal for Numerical Methods in Fluids*, Vol. 90, No. 2, 2019, pp. 81–113.

[23] Spalart, P., and Allmaras, S., "A one-equation turbulence model for aerodynamic flows," *30th Aerospace Sciences Meeting and Exhibit*, AIAA 1992-439, 1992.

[24] Roe, P. L., "Approximate Riemann solvers, parameter vectors, and difference schemes," *Journal of Computational Physics*, Vol. 43, No. 2, 1981, pp. 357–372.

[25] Bassi, F., and Rebay, S., "GMRES discontinuous Galerkin solution of the compressible Navier-Stokes equations," *Discontinuous Galerkin Methods*, Springer, 2000, pp. 197–208.

[26] Nguyen, N., Persson, P.-O., and Peraire, J., "RANS solutions using high order discontinuous Galerkin methods," *45th AIAA Aerospace Sciences Meeting and Exhibit*, AIAA 2007-914, 2007.